8 Operational Atmospheric Correction of MODIS Visible to Middle Infrared Land Surface Data in the Case of an Infinite Lambertian Target

Eric F. Vermote and Nazmi Z. Saleous

8.1 Introduction

The atmospheric correction of remote sensing data has always been a concern to the ocean color community, where the signal of interest is almost an order of magnitude smaller than the top of the atmosphere signal. The first data over ocean were corrected for gases, molecular and aerosol effect (Gordon et al., 1983). Atmospheric correction over ocean on SeaWiFS, MODIS and MERIS is now including correction for gaseous effect, an inversion of the aerosol type and amount using the near infrared bands (0.76 μm and 0.87 μm) and accounts for the coupling of the sun-glint directional reflectance with the atmosphere. Typically, over open water the accuracy of those corrections is of the order of 10% – 30% of the reflectance in the blue band (0.412 μm and 0.450 μm), which typically represents 4.10^{-3} to 1.10^{-2} absolute reflectance unit under low aerosol loading (typically optical thickness of 0.2). However, over coastal areas, the assumption that the water contribution is in 0.76 μm and 0.87 μm is no longer valid, due to the contributions of sediments. The atmospheric correction for coastal areas can only be achieved on a case by case basis and with variable accuracy.

Over land, because of the lesser impact of the atmosphere compared to ocean, and the lack of dedicated mission (AVHRR was a meteorological satellite and Thematic Mapper was mainly used in land cover studies), the use of standard atmospheric correction procedure has been slower to establish and indices and procedures to minimize atmospheric effect have been widely used. With the design and development of the Earth Observing System mission, atmospheric correction has been prototyped over land for AVHRR (Jasmes and Kallur, 1994; El Saleous et al., 2000), Thematic Mapper (Ouaidrari and Vermote, 1999) and SeaWiFS (Vermote el al., 2001). Dedicated algorithms for retrieval of aerosol over land for MODIS (Kaufman et al., 1997) and MISR (Martonchik et al., 1997) and algorithms for atmospheric correction, which take into account gases, molecular and aerosol effects, as well as surface Bidirectional Reflectance Distribution Function (BRDF) atmosphere, have been designed, documented and evaluated in the pre-launch phase (Vermote et al., 1997; Martonchik et al., 1997).

In the first phase of the mission, an initial validation and evaluation of the MODIS algorithm (Lambertian assumption) on a global basis has been performed and the accuracy established to be 5.10^{-4} or 5% relative accuracy, whichever is greater, under low aerosol optical thickness.

The chaprer describes the operational procedure for atmospheric correction over land in the case of the infinite Lambertian target. It starts first with a theoretical background section and then shows how the solution of the equation of transfer is implemented in operations, a section is devoted to the input of the atmospheric corrections, and the last section discusses the error budget and validation.

8.2 Theoretical Background

Using the formalism developed for the 5S code, the solution of the radiation transfer equation, corresponding to the problem illustrated by Fig. 8.1(a) and employing the Lambertian Uniform Target assumption for observation in spectral band *i*, assuming a standard atmospheric profile, but variable, pressure (P), ozone and water vapor amount ($U_{\mathrm{O_3}}, U_{\mathrm{H_2O}}$), is written as (Vermote et al., 1997):

$$\rho^i_{\mathrm{TOA}}(\theta_{\mathrm{s}}, \theta_{\mathrm{v}}, \phi, P, \overbrace{\tau^i_{\mathrm{A}}, \omega^i_0, P^i_{\mathrm{A}}}^{Aer^i}, U_{\mathrm{H_2O}}, U_{\mathrm{O_3}}) =$$

$$T^i_{\mathrm{g_{OG}}}(m,P)T^i_{\mathrm{g_{O_3}}}(m,U_{U_{\mathrm{O_3}}})\left[\begin{array}{l}\rho^i_{\mathrm{atm}}(\theta_{\mathrm{s}}, \theta_{\mathrm{v}}, \phi, P, Aer^i, U_{\mathrm{H_2O}}) \\ +Tr^i_{\mathrm{atm}}(\theta_{\mathrm{s}}, \theta_{\mathrm{v}}, P, Aer^i)\dfrac{\rho_{\mathrm{S}}}{1-S^i_{\mathrm{atm}}(P, Aer^i)\rho_{\mathrm{S}}}T^i_{\mathrm{g_{H_2O}}}(m,U_{U_{\mathrm{H_2O}}})\end{array}\right]$$

(8.1)

Where ρ_{TOA} = the reflectance at the top of the atmosphere;

T_{g} = the gaseous transmission by water vapor, $T_{\mathrm{g_{H_2O}}}$, by ozone, $T_{\mathrm{g_{O_3}}}$, or other gases, $T_{\mathrm{g_{OG}}}$ (e.g. CO_2…);

ρ_{atm} = the atmosphere intrinsic reflectance;

Tr_{atm} = the total atmosphere transmission (downward and upward);

S_{atm} = the atmosphere spherical albedo; and

ρ_{S} = the surface reflectance to be retrieved by the atmospheric correction procedure.

The geometrical conditions are described by θ_{s}, the solar zenith angle, θ_{v}, the view zenith angle and ϕ, the difference between the solar and view azimuth angle, P is the pressure which influences the number of molecules in the atmosphere and the concentration of absorbing gases.

τ_A, ω_0 and P_A describe the aerosol properties and are spectrally dependent, τ_A is the aerosol optical thickness, ω_0 is the aerosol single scattering albedo, describing the absorption of the aerosol, ω_0 is equal to 1 for non-absorption particles and 0 for completely absorbing particles.

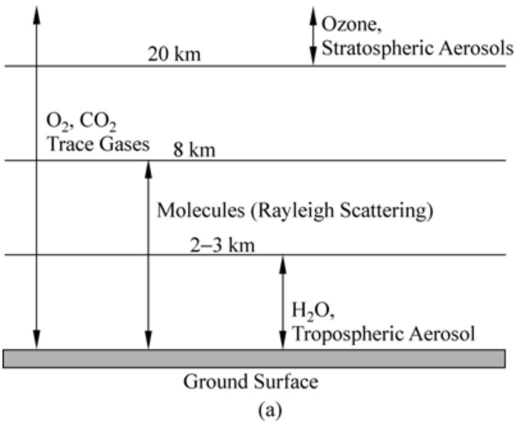

Figure 8.1(a) The atmospheric components affecting the remote sensing signal in the 0.4 – 2.5 μm range

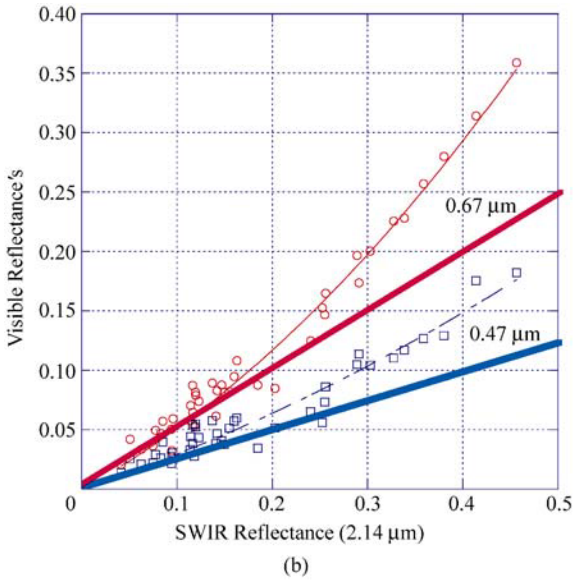

Figure 8.1(b) Empirical relationship between the visible and short wave infrared reflectance's observed over 40 sun-photometer sites a variety of land cover type and distributed globally

P_{A} is the aerosol phase function, $U_{\mathrm{H_2O}}$ is the integrated water vapor content, $U_{\mathrm{O_3}}$ is the integrated ozone content, *m* is the air-mass computed as 1/cos (θ_{s}) + 1/cos(θ_{v}).

The effect of the water vapor on the atmosphere intrinsic reflectance is approximated in 6S code as:

$$\rho^{i}_{\mathrm{atm}}(\theta_{\mathrm{s}},\theta_{\mathrm{v}},\phi,P,Aer^{i},U_{\mathrm{H_2O}})$$
$$=\rho^{i}_{\mathrm{R}}(\theta_{\mathrm{s}},\theta_{\mathrm{v}},\phi,P)+\left(\rho^{i}_{\mathrm{R+Aer}}(\theta_{\mathrm{s}},\theta_{\mathrm{v}},\phi,P,Aer^{i})-\rho^{i}_{\mathrm{R}}(\theta_{\mathrm{s}},\theta_{\mathrm{v}},\phi,P)\right)T^{i}_{\mathrm{g_{H_2O}}}\left(m,\frac{U_{U_{\mathrm{H_2O}}}}{2}\right) \tag{8.2}$$

where ρ_{R} represents the reflectance of the atmosphere due to molecular (Rayleigh) scattering, and $\rho_{\mathrm{R+Aer}}$ represents the reflectance of the mixing molecule and aerosol, which is computed in 6S using the successive order of scattering method. Accounting correctly for the mixing and the so-called coupling effect (Deschamps et al., 1983) is important for achieving high accuracy in the modeling of atmospheric effect. This approximation conserves the correct computation of the coupling, and supposes that the water vapor is mixed with aerosol and that the molecular scattering is not affected by the water vapor absorption. This approximation is reasonable in most cases where observation bands are narrow and there is no strong absorption by the water vapor, as it is the case for surface remote sensing bands.

The total atmosphere transmission, T_{r}, is further decomposed into a downward and an upward term, which are respectively dependent on θ_{s} and θ_{v} and are computed using the same function by virtue of the reciprocity principle, that is:

$$Tr^{i}_{\mathrm{atm}}(\theta_{\mathrm{s}},\theta_{\mathrm{v}},P,Aer^{i})=T^{i}_{\mathrm{atm}}(\theta_{\mathrm{s}},P,Aer^{i})T^{i}_{\mathrm{atm}}(\theta_{\mathrm{v}},P,Aer^{i}) \tag{8.3}$$

8.3 Operational Implementation

8.3.1 Simplification to Account for Surface Pressure

For the computer code, the functions related to atmospheric scattering and absorption, ρ_{atm}, T_{atm} and S_{atm} can be computed by interpolation from a pre-computed lookup table because they can not be simply modeled. The gaseous transmission function can be written in MODIS or VIIRS bands as simple analytical function. The molecular reflectance term can be computed very efficiently using a semi-empirical approach based on the decomposition suggested by Chandrasekhar, which is described in details in Vermote and Tanr’e (1992).

Using a subsequent approximation, we can further simplify the dependence of the key term on the pressure, by only computing $\rho_{\mathrm{R+Aer}}$ at standard pressure, P_0, enabling us to substantially reduce the dimension of the lookup tables, that is:

$$\rho^i_{\mathrm{atm}}(\theta_{\mathrm{s}},\theta_{\mathrm{v}},\phi,P,Aer^i,U_{\mathrm{H_2O}})$$
$$=\rho^i_{\mathrm{R}}(\theta_{\mathrm{s}},\theta_{\mathrm{v}},\phi,P)+\left(\rho^i_{\mathrm{R+Aer}}(\theta_{\mathrm{s}},\theta_{\mathrm{v}},\phi,P_0,Aer^i)-\rho^i_{\mathrm{R}}(\theta_{\mathrm{s}},\theta_{\mathrm{v}},\phi,P_0)\right)T^i_{\mathrm{g_{H_2O}}}\left(m,\frac{U_{U_{\mathrm{H_2O}}}}{2}\right) \tag{8.4}$$

The same approach could be applied to the transmission term, that is:

$$T^i_{\mathrm{atm}}(\theta,P,Aer^i)=T^i_{\mathrm{atm}}(\theta,P_0,Aer^i)\frac{T^i_{\mathrm{R}}(\theta,P)}{T^i_{\mathrm{R}}(\theta,P_0)} \tag{8.5}$$

where T_{R} is the atmosphere transmission function due to molecular scattering.

8.3.2 Detailed Computations

The code implements the equations detailed in (8.1) – (8.5), using a lookup table approach and analytic expression. The following section details the computation of each term in the computer code.

8.3.2.1 $T^i_{\mathrm{g_{OG}}}(m,P)$—Gaseous Transmission by Other Gases

The gaseous transmission by gases other than water or ozone in each spectral band can be written as a function of the air mass, *m*, and the pressure *P* (in atm), as:

$$T^i_{\mathrm{g_{OG}}}(m,P)=\exp\left[\begin{array}{l}m\left(a^i_0P+a^i_1\mathrm{Log}(P)\right)\\+\mathrm{Log}(m)\left(b^i_0P+b^i_1\mathrm{Log}(P)\right)+m\mathrm{Log}(m)\left(c^i_0P+c^i_1\mathrm{Log}(P)\right)\end{array}\right] \tag{8.6}$$

8.3.2.2 $T^i_{\mathrm{g_{O_3}}}(m,U_{\mathrm{O_3}})$—Ozone Gaseous Transmission

The ozone gaseous transmission in the narrow bands (in the Chappuis band) could be simply modeled as:

$$T^i_{\mathrm{g_{O_3}}}(m,U_{\mathrm{O_3}})=e^{-ma^i_{\mathrm{O_3}}U_{\mathrm{O_3}}} \tag{8.7}$$

8.3.2.3 $T^i_{\mathrm{g_{H_2O}}}(m,U_{\mathrm{H_2O}})$—Water Vapor Gaseous Transmission

The water vapor transmission is modeled as:

$$T^i_{\mathrm{g_{H_2O}}}(m,U_{\mathrm{H_2O}})=\exp\left[\begin{array}{l}a^i_{\mathrm{H_2O}}mU_{\mathrm{H_2O}}\\+b^i_{\mathrm{H_2O}}\mathrm{Log}(mU_{\mathrm{H_2O}})+c^i_{\mathrm{H_2O}}mU_{\mathrm{H_2O}}\mathrm{Log}(mU_{\mathrm{H_2O}})\end{array}\right] \tag{8.8}$$

8.3.2.4 $\rho_{\mathrm{R}}^{i}(\theta_{\mathrm{s}},\theta_{\mathrm{v}},\phi,P_0)$ —Molecular Atmospheric Reflectance at Standard Pressure

This quantity is computed by the 6S subroutine CHAND.f , described in Vermote et al. (1992), which accepts as direct input the geometrical conditions $(\mu_{\mathrm{s}},\mu_{\mathrm{v}},\phi)$, where μ_{s} (resp. μ_{v}) is the cosine of the solar (resp. view) zenith angle, and ϕ the relative azimuth and the molecular optical thickness in that case at standard pressure, τ_{R}, which is pre-computed (by 6S).

8.3.2.5 $\rho_{\mathrm{R}}^{i}(\theta_{\mathrm{s}},\theta_{\mathrm{v}},\phi,P_0)$ —Molecular Atmospheric Reflectance at Actual Pressure

The adjustment is simply done by adjusting the amount of molecules or the molecular optical thickness, according to:

$$\tau_{\mathrm{R}}(P) = P\tau_{\mathrm{R}} \tag{8.9}$$

The pressure, *P*, is expressed in atmospheres.

8.3.2.6 $\rho_{\mathrm{R+Aer}}^{i}(\theta_{\mathrm{s}},\theta_{\mathrm{v}},\phi,P_0,Aer^{i})$ —Intrinsic Reflectance at Standard Pressure

This quantity is pre-computed by 6S in a lookup table for each band and each aerosol model $(P_{\mathrm{A}},\omega_0)$. The step in solar zenith angle is 4 deg, in view angle 4 deg corresponding to the gauss quadrature of 24 angles (with the nadir added), the step is kept constant in scattering angle (4 degree), Θ, defined as:

$$\cos(\Theta) = -\cos(\theta_{\mathrm{s}})\cos(\theta_{\mathrm{v}}) - \cos(\phi)\sin(\theta_{\mathrm{s}})\sin(\theta_{\mathrm{v}}) \tag{8.10}$$

Resulting in a variable number of steps is for each θ_{s}, θ_{v} configuration. The indexing to the correct values in the lookup table is achieved through the use of the ANGLE lookup table, which keeps track of the number of azimuth angles computed for each θ_{s}, θ_{v} configuration. Though, more expensive and more complicated to interpolate within, this structure achieves a higher precision with a reduced size lookup table, for a term for which accuracy is critical to the atmospheric correction.

The step in aerosol optical depth is variable to optimize the performance of the correction with the error induced by the interpolation (i.e. finer a low optical depth).

8.3.2.7 $T_{\mathrm{atm}}^{i}(\theta,P_0,Aer^{i})$ —Atmosphere Transmission on at Standard Pressure

This quantity is pre-computed in 6S by using the successive order of scattering method and illuminating the bottom of the layer with isotropic light. The code accounts for the mixing of aerosol molecules within the atmosphere. The values are computed with a step of 4 deg in θ and for each aerosol model and each band for predefined values of τ_{A}. The interpolation for any θ and τ is relatively straightforward since this table has only 2 dimensions. The table volume is also very modest.

8.3.2.8 $T_{\mathrm{R}}^{i}(\theta, P_0)$—Molecular (Rayleigh) Transmission at Standard Pressure

The molecular transmission at standard pressure is computed using the value of molecular optical depth at standard pressure, τ_{R}. Using the two stream method, the molecular transmission could be approximated by:

$$T_{\mathrm{R}}^{i}(\theta, P_0) = \frac{\lfloor 2/3 + \cos(\theta) \rfloor + \lfloor 2/3 - \cos(\theta) \rfloor \mathrm{e}^{-\tau_{\mathrm{R}}/\cos(\theta)}}{4/3 + \tau_{\mathrm{R}}} \tag{8.11}$$

8.3.2.9 $T_{\mathrm{R}}^{i}(\theta, P)$—Molecular (Rayleigh) Transmission on at Actual Pressure

Using the same method as in Molecular Atmospheric Reflectance at Standard Pressure we simply replace, in Eq. (8.9), τ_{R} with $\tau_{\mathrm{R}}(P)$ (Eq. (8.7)).

8.3.2.10 Atmosphere Spherical Albedo at Actual Pressure

The atmospheric spherical albedo at actual pressure, $S_{\mathrm{atm}}^{i}(P, Aer^{i})$, is described as:

$$S_{\mathrm{atm}}^{i}(P, Aer^{i}) = \int_0^{\pi/2} \int_0^{\pi/2} \int_0^{2\pi} \rho_{\mathrm{atm}}^{i}(\theta, \theta', \phi, P, Aer^{i}) \sin(\theta) \cos(\theta') \mathrm{d}\theta \mathrm{d}\theta' \mathrm{d}\phi \tag{8.12}$$

By ignoring the water vapor dependence on the atmosphere intrinsic reflectance (S acting as a second order effect), we can write the same relation we have written for the atmosphere intrinsic reflectance, that is

$$S_{\mathrm{atm}}^{i}(P, Aer^{i}) = (S_{\mathrm{atm}}^{i}(P_0, Aer^{i}) - S_{\mathrm{R}}^{i}(P_0)) + S_{\mathrm{R}}^{i}(P) \tag{8.13}$$

So the $S_{\mathrm{atm}}^{i}(P_0, Aer^{i})$ is stored in a pre-calculated lookup table depending only on aerosol optical depth and model. The $S_{\mathrm{R}}^{i}(P)$ term is computed by an analytic expression based on the integral of Eq. (8.11) that is:

$$S_{\mathrm{R}}^{i}(P) = \frac{1}{4 + 3\tau_{\mathrm{R}}} \left[3\tau_{\mathrm{R}} - 4E_3(\tau_{\mathrm{R}}) + 6E_4(\tau_{\mathrm{R}}) \right] \tag{8.14}$$

where E_3 and E_4 are exponential integral function (see 6S code for details; Vermote et al., 1997).

8.4 Input and Ancillary Data

The atmospheric correction approach described in Sections 8.2 and 8.3 requires key atmospheric parameters: surface pressure, ozone concentration, column water vapor and aerosol optical thickness. The surface pressure and ozone concentration are slow varying parameters both spatially and temporally. They can be estimated from the coarse resolution meteorological data. We recommend using an interpolation scheme in the temporal and spatial space to determine these parameters at the acquisition time and spatial resolution.

In general, the water vapor content and aerosols vary strongly in time and space. Where possible, they should be derived from data acquired by the same instrument for which the atmospheric correction is performed, or an instrument flying on the same platform. In the case of the MODIS surface reflectance, these parameters are derived from MODIS calibrated data.

8.4.1 Surface Pressure

The surface pressure (*P*) is used to compute the Rayleigh optical thickness. A primary source of surface pressure meteorological data is the National Center for Environmental Prediction (NCEP) Global Data Assimilation System (GDAS) where the surface pressure parameter is produced at a spatial resolution of 1×1 degree every 6 hours. These data are available for the period 1948 – present. The real-time data can be obtained from NCEP's FTP site (ftp.ncep.noaa.gov) and historical data can be ordered from the National Center for Atmospheric Research (NCAR) (http://dss.ucar.edu).

Other sources of a 1×1 degree surface pressure field include the National Aeronautics and Space Agency's (NASA) Global Modeling and Assimilation Office (GMAO) (http://gmao.gsfc.nasa.gov) and the European Center for Medium-Range Weather Forecast (ECMWF) where these data are available for the period 1958 – present (http://www.ecmwf.int).

The coarse spatial resolution of the meteorological data does not match the higher spatial variability of the surface pressure due to terrain elevation. To increase the spatial resolution of the surface pressure field, we use a Digital Elevation Model (DEM) to map the surface pressure at a higher resolution within each meteorological data grid cell. The GTOPO30 DEM is available globally at a resolution of 30 arc seconds (approximately 1 km) (http://edcdaac.usgs.gov/ gtopo30/ gtopo30.asp). To increase the resolution within a meteorological data grid cell where the surface pressure is P_{meteo}, we determine the set of DEM pixels that intersect the grid cell and compute for each pixel the standard pressure P^{i}_{DEM} where:

$$P^{i}_{\text{DEM}}(\text{millibar}) = 1,013 \square \frac{\text{Elevation(km)}}{8} \tag{8.15}$$

The ratio of P_{meteo} and the average pressure derived from the selected DEM pixels $\left(\left\langle P_{\text{DEM}} \right\rangle\right)$ is used to adjust the pressure at the DEM resolution. We assumed that the accuracy on the final pressure is 10 millibars.

8.4.2 Ozone

The ozone concentration is primarily obtained from the NASA's Total Ozone

Mapping Spectrometer (TOMS). These data are available daily at a spatial resolution of 1×1 degree for the period 1979 – present and can be obtained from the TOMS Website at http://toms.gsfc.nasa.gov. The nominal uncertainty of this product reported on the TOMS Web page is 3% – 4% (http://toms.gsfc.nasa.gov/eptoms/dataqual/nominal.html).

Alternatively, the National Oceanic and Atmospheric Administration's (NOAA) Total Operational Vertical Sounder (TOVS) ozone product available from NOAA's Climate Prediction Center (CPC) (http://www.cpc.ncep.noaa.gov/products/stratosphere/tovsto/) can be used.

8.4.3 Water Vapor

Where possible, the column water vapor should be derived from the instrument where atmospheric correction is performed. In the case of the MODIS instrument for example, the near-infrared bands 18 (931 – 941 nm) and 19 (915 – 965 nm) are used to retrieve the column water vapor content. The approach based on the two-band ratio is described by Gao (Gao and Kaufman, 2003). This approach determines the instantaneous water vapor content at the time of acquisition with an accuracy of 5% – 10%. Alternatively, meteorological data from NCEP GDAS can be used.

8.4.4 Aerosol Optical Thickness

The approach to aerosol optical thickness retrieval over land is based on the "dark and dense vegetation (DDV)" technique introduced by Holben et al. (1992). It is based on using an empirical relationship between the surface reflectance in the shortwave visible bands (where the aerosol effect is strong and the surface signal is low) and in the shortwave infrared bands (where the aerosol effect is negligible) to predict the surface reflectance in the visible bands. Such a relation has been used for different instruments. Ouaidrari and Vermote (1999) estimated the surface reflectance of dark target in Landsat's Band 1 (490 nm) to be 1/3 of the reflectance in band 7 (2.19 μm). El Saleous et al. (2000) estimated the surface reflectance in AVHRR's band 1 (670 nm) using the reflective component of band 3 (3.75 μm).

The original approach suggested using a linear relationship limited in scope to dark targets. Using a set of 40 AERONET sites representative of different land covers; we derived a non-linear relationship that can be applied to brighter targets. Figure 8.1(b) shows plots of the surface reflectance in blue and red bands (470 and 650 nm) as a function of shortwave infrared (SWIR) reflectance (2,130 nm) for surface with a SWIR reflectance up to 0.5. To compute the estimated surface reflectance in the blue and red bands, the relationship in Fig. 8.1(b) is applied to the reflectance in band 7 (2,130 nm) after it has been corrected for atmospheric effects.

Using the surface reflectance estimate in the blue and red bands, the estimated top of the atmosphere reflectance at the observation geometry ($\rho^{i}_{\mathrm{TOA\_est}}(\theta_{\mathrm{s}},\theta_{\mathrm{V}},\phi,Aer^{i})$) is computed using Equations (8.1) – (8.4) and the intrinsic atmospheric reflectance ($\rho^{i}_{\mathrm{R+Aer}}(\theta_{\mathrm{s}},\theta_{\mathrm{V}},\phi,P_{0},Aer^{i})$ and atmospheric transmission ($T^{i}_{\mathrm{atm}}(\theta,P_{0},Aer^{i})$, described in Sections 8.3.2.6 and 8.3.2.7. $\rho^{i}_{\mathrm{TOA\_est}}(\theta_{\mathrm{s}},\theta_{\mathrm{V}},\phi,Aer^{i})$ is computed for all the optical thickness values included in the 6S lookup tables. The values of the estimated TOA reflectance bracketing the observed TOA reflectance ($\rho^{i}_{\mathrm{TOA\_est}}(\theta_{\mathrm{s}},\theta_{\mathrm{V}},\phi,Aer^{i}_{1})$ and $\rho^{i}_{\mathrm{TOA\_est}}(\theta_{\mathrm{s}},\theta_{\mathrm{V}},\phi,Aer^{i}_{2})$) are identified and the aerosol optical thickness (Aer^{i}) is computed by linear interpolation.

8.5 Application to MODIS Data and Error Budget

The previously described algorithm has been applied to the MODIS instrument on-board the Terra (morning) and Aqua (afternoon) satellites. In that case, the retrieval of the water vapor integrated content and the aerosol optical thickness is performed using the remotely sensed data themselves using the 1-km resolution bands that enable the capture of spatial and temporal variability of those inputs. In order to examine the impact of the atmospheric effect on the MODIS land bands and estimate the accuracy of the atmospheric correction under several scenarios, we have selected three typical land covers, a forest type, a savanna and a semi arid surface. The data have been acquired by MODIS at a sun-photometer site on a day where the optical thickness was low; the correction of the level-1B data has been performed using 6S and the sun-photometer measurements (optical thickness, size distribution and refractive indices). The data have been slightly adjusted in Bands 1 (645 nm) and 3 (470 nm) to agree with the empirical relationship used for the aerosol retrieval algorithm, the error on the atmospheric correction algorithm by uncertainties in that relationship will be addressed later in this section (8.5.5).

For a variety of atmosphere and geometrical conditions (see Table 8.1(a)) the signals at the top of the atmosphere have been simulated for the three sites using the 6S radiative transfer code (Vermote et al., 1997). Figures 8.2(a) – 8.2(c) show the surface reflectance for the three sites as a function of the central wavelength of each of the seven MODIS land bands. The atmospheric impact is strong in all the bands due to the fact that all of the ranges of the aerosol models have been considered in this simulation (see Table 8.1(b)), based on the climatology established by Dubovik et al. (2002). The atmospheric effect is considerably larger at short wavelength, especially with respect to the ground surface reflectance, which is definitely to our advantage since we are using those wavelengths to retrieve aerosol properties.

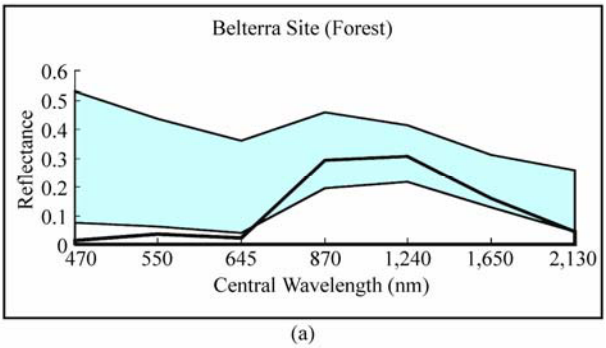

Figure 8.2(a) Surface reflectance at the Belterra site (forest) for each of the seven MODIS bands (thick line), the blue area represents the variability in the signal at the top of the atmosphere encountered by simulating the conditions described in Table 8.1

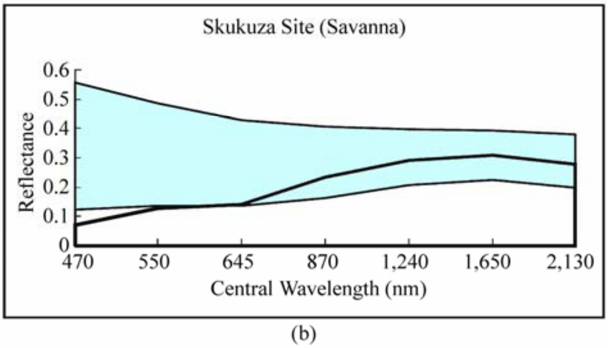

Figure 8.2(b) Surface reflectance at the Skukuza site (savanna) for each of the seven MODIS bands (thick line), the blue area represents the variability in the signal at the top of the atmosphere encountered by simulating the conditions described in Table 8.1

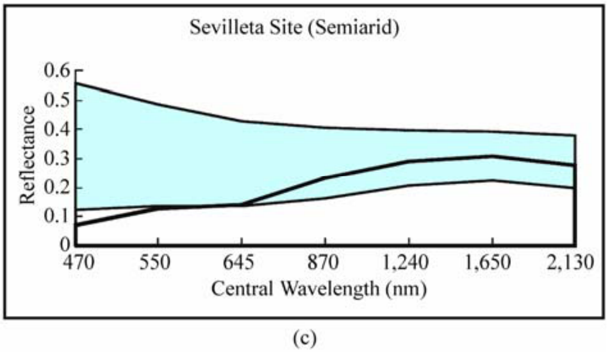

Figure 8.2(c) Surface reflectance at the Sevilleta site (semiarid) for each of the seven MODIS bands (thick line), the blue area represents the variability in the signal at the top of the atmosphere encountered by simulating the conditions described in Table 8.1

Table 8.1(a) Description of the different parameter set used to generate the top of the atmosphere reflectances and compute the uncertainties in the corrected surface reflectances

<table>
<tr><th>Parameter</th><th>Values</th></tr>
<tr><td>Geometrical Conditions</td><td>
<table>
<tr><th>Solar Zenith</th><th>View Zenith</th><th>Relative Azimuth</th><th>Case Name</th></tr>
<tr><td>30</td><td>0</td><td>0</td><td>A</td></tr>
<tr><td>30</td><td>30</td><td>0</td><td>B</td></tr>
<tr><td>30</td><td>30</td><td>180</td><td>C</td></tr>
<tr><td>30</td><td>60</td><td>0</td><td>D</td></tr>
<tr><td>30</td><td>60</td><td>180</td><td>E</td></tr>
<tr><td>60</td><td>0</td><td>0</td><td>F</td></tr>
<tr><td>60</td><td>30</td><td>0</td><td>G</td></tr>
<tr><td>60</td><td>30</td><td>180</td><td>H</td></tr>
<tr><td>60</td><td>60</td><td>0</td><td>I</td></tr>
<tr><td>60</td><td>60</td><td>180</td><td>J</td></tr>
</table>
</td></tr>
<tr><td>Aerosol Optical Depth</td><td>0.05 (clear) 0.30 (average) 0.50 (high)</td></tr>
<tr><td>Aerosol Model</td><td>urban clean, urban polluted, smoke low absorption smoke high absorption (see Table 8.1(b) for details)</td></tr>
<tr><td>Water Vapor Content (g/cm^2)</td><td>1.0, 3.0 and 5.0 uncertainties +/– 0.2</td></tr>
<tr><td>Ozone Content ($cm \cdot atm$)</td><td>0.25, 0.3, 0.35 uncertainties +/– 0.02</td></tr>
<tr><td>Pressure (mb)</td><td>1,013 mb, 930 mb, 845 mb uncertainties +/– 10</td></tr>
</table>

Table 8.1(b) Description of the characteristics of the aerosol model used in the study (based on the climatology of Dubovik et al. (2002))

		Aerosol model			
		Urban Clean	Urban Polluted	Smoke Low Absorption	Smoke High Absorption
Refractive Index	Real	$1.41 - 0.03\,\tau_{440\text{ nm}}$	1.47	1.47	1.51
	Imaginary	0.003	0.014	0.0093	0.021
Small Particle Mode	Volume Mean Radius (μm)	$0.12 + 0.11\,\tau_{440\text{ nm}}$	$0.12 + 0.04\,\tau_{440\text{ nm}}$	$0.13 + 0.04\,\tau_{440\text{ nm}}$	$0.12 + 0.025\,\tau_{440\text{ nm}}$
	Standard Deviation	0.38	0.43	0.40	0.40
	Volume Concentration ($\mu m^3/\mu m^2$)	$0.15\,\tau_{440\text{ nm}}$	$0.12\,\tau_{440\text{ nm}}$	$0.12\,\tau_{440\text{ nm}}$	$0.12\,\tau_{440\text{ nm}}$

Continued

		Aerosol model			
		Urban Clean	Urban Polluted	Smoke Low Absorption	Smoke High Absorption
Coarse Particle Mode	Volume Mean Radius (μm)	3.03+0.49 $\tau_{440\ \mathrm{nm}}$	2.72+0.60 $\tau_{440\ \mathrm{nm}}$	3.27+0.58 $\tau_{440\ \mathrm{nm}}$	3.22+0.71 $\tau_{440\ \mathrm{nm}}$
	Standard Deviation	0.75	0.63	0.79	0.73
	Volume Concentration ($\mu m^3/\mu m^2$)	0.01+0.04 $\tau_{440\ \mathrm{nm}}$	0.11 $\tau_{440\ \mathrm{nm}}$	0.05 $\tau_{440\ \mathrm{nm}}$	0.09 $\tau_{440\ \mathrm{nm}}$

The rest of this section presents, in detail, the impact of the sources of uncertainties, calibration, ozone and water vapor content, pressure, the relationship between the 2,130 nm and 470 nm, 645 nm bands, as well as the aerosol type, which is not inverted by the procedure which relies on a prescribed model (urban clean) and adjust the spectral dependence of the actual aerosol by using retrieval at both 470 nm and 645 nm. As a theoretical error budget, the precision is only indicative of the potential accuracy of the product and needs to be verified by independent validation (see Section 8.5.7).

8.5.1 Calibration Uncertainties

We ran a set of simulations for three different optical thicknesses (0.05:clear; 0.30:avg; 0.50:high), using the urban clean model, for an average content in water vapor and ozone at standard pressure for the 10 geometrical conditions (a through *j*), for each of the three different sites. We simulated an error of +2% and –2% in the absolute calibration across all the seven MODIS bands. The results of the simulations are summarized in Tables 8.2(a) – 8.2(c), where we report the maximum and minimum absolute error encountered as a function of aerosol optical thickness, we report the geometrical conditions at which that maximum or minimum occurred.

We also report the average error for all the geometrical conditions which will be used later when we are summing all the uncertainties. The error increases with the increase in optical thickness and the maximum error occurs where the atmospheric effects are the strongest (case *i*, sun and view at 60 deg in the backscattering directions). Generally, the overall error stays under 2% in relative for all optical thicknesses considered and does not amplified the error sources. It is true that a similar error across all wavelengths is probably favorable, but it is also representing the most likely error for MODIS which intra bands for the land bands is probably better than 2% due to the use of the solar diffuser and solar diffuser stability monitor in the calibration process. Also presented in Fig. 8.3 is the error on the retrieved optical thickness given the error on calibration.

Table 8.2(a) Error on the surface reflectance ($\times$ 10,000) due to uncertainties in the absolute calibration ($\pm 2\%$) for the Belterra site

Central Wavelength (nm)		470	550	645	870	1,240	1,650	2,130
Surface Reflectance $\times$ 10,000		120	375	240	2,931	3,083	1,591	480
Maximum Error $\times$ 10,000	Clear	0008j	0010i	0015i	0077i	0084i	0078i	0083i
	Avg.	0009i	0012d	0027i	0090i	0085i	0062i	0044i
	High	0012d	0013i	0047i	0112i	0106i	0089i	0071i
Minimum Error $\times$ 10,000	Clear	0003c	0005j	0005c	0059a	0059f	0031c	0014c
	Avg.	0000e	0004j	0002j	0060c	0061c	0032c	0011c
	High	0003f	0003e	0007c	0062c	0062c	0033c	0012c
Average Error $\times$ 10,000	Clear	4	7	7	62	65	44	34
	Avg.	2	8	10	67	66	39	19
	High	7	8	16	76	72	46	27

Table 8.2(b) Error on the surface reflectance ($\times$ 10,000) due to uncertainties in the absolute calibration ($\pm 2\%$) for the Skukuza site

Central Wavelength (nm)		470	550	645	870	1,240	1,650	2,130
Surface Reflectance $\times$ 10,000		400	636	800	2,226	2,880	2,483	1,600
Maximum Error $\times$ 10,000	Clear	0013j	0013b	0024i	0065i	0080i	0080i	0080i
	Avg.	0015i	0015i	0030i	0074i	0079i	0070i	0054i
	High	0013d	0011a	0049i	0101i	0098i	0088i	0071i
Minimum Error $\times$ 10,000	Clear	0008a	0009j	0016c	0045c	0056f	0048f	0031f
	Avg.	0006c	0004j	0016c	0046c	0058c	0049c	0032c
	High	0001e	0005j	0018c	0048c	0058c	0050c	0032c
Average Error $\times$ 10,000	Clear	9	11	17	49	61	56	45
	Avg.	8	11	19	53	63	54	37
	High	6	9	24	63	68	59	42

Table 8.2(c) Error on the surface reflectance ($\times$10,000) due to uncertainties in the absolute calibration ($\pm$2%) for the Sevilleta site

Central Wavelength (nm)		470	550	645	870	1,240	1,650	2,130
Surface Reflectance $\times$10,000		700	1,246	1,400	2,324	2,929	3,085	2,800
Maximum Error $\times$10,000	Clear	0019j	0026i	0033i	0062i	0077i	0081i	0080i
	Avg.	0021i	0030i	0039i	0067i	0075i	0074i	0070j
	High	0017a	0040d	0046i	0086i	0090j	0086j	0081j
Minimum Error $\times$10,000	Clear	0014a	0021j	0027j	0047a	0058c	0061c	0055c
	Avg.	0012e	0017j	0028c	0048a	0059a	0062a	0056a
	High	0006e	0014j	0029a	0049a	0059c	0061c	0055c
Average Error $\times$10,000	Clear	14	24	28	49	61	65	61
	Avg.	14	25	30	53	63	64	58
	High	12	24	32	60	67	67	60

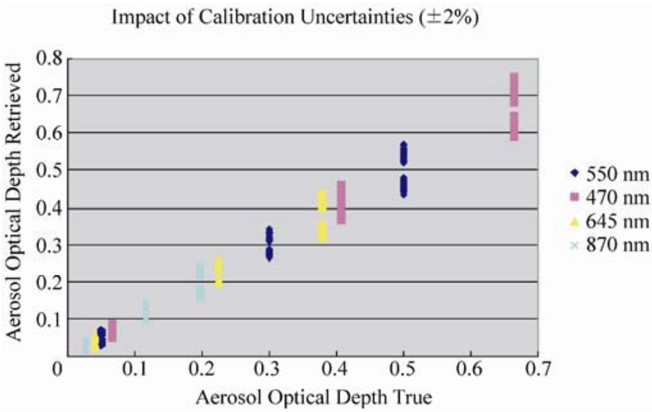

Figure 8.3 Comparison of the optical depth at 470 nm, 550 nm, 645 nm and 870 nm retrieved and input in the simulation for the 9 geometries given in Table 8.2 for an error of calibration of $\pm$2%

8.5.2 Uncertainties on Ancillary Data Pressure

We ran a set of simulations at three different pressures, 1,013 mb, 930 mb, and 845 mb, with a variation of 10 mb for each case for an optical depth of 0.3. The three different pressures represent sites at altitude of 0 m, 700 m and 1,500 m. Tables 8.3(a) – 8.3(c) report the error in each band for the three different sites. The pressure error will influence the molecular scattering term and also the concentration of trace gases that might be affecting a specific band. However the aerosol optical thickness is also affected by the uncertainty on surface pressure (see Fig. 8.4), in such a way that eventually all the bands become affected.

Table 8.3(a) Error on the surface reflectance ($\times$ 10,000) due to uncertainties in the surface pressure ($\pm$10 mb) for the Belterra site

Central Wavelength (nm)		470	550	645	870	1,240	1,650	2,130
Surface Reflectance $\times$ 10,000		120	375	240	2,931	3,083	1,591	480
Maximum Error $\times$ 10,000	Clear	0003i	0001e	0009i	0008i	0007i	0011i	0012i
	Avg.	0003i	0001e	0008i	0008i	0007i	0011i	0011j
	High	0002i	0001e	0008i	0008i	0007i	0010i	0011i
Minimum Error $\times$ 10,000	Clear	0000c	0000a	0000c	0000a	0000a	0000c	0000c
	Avg.	0000c	0000a	0000c	0000a	0000a	0000c	0000c
	High	0000a	0000a	0000c	0000a	0000a	0000a	0000c
Average Error $\times$ 10,000	Clear	1	0	2	1	0	2	2
	Avg.	1	0	1	1	0	1	2
	High	0	0	1	1	0	1	2

Table 8.3(b) Error on the surface reflectance ($\times$ 10,000) due to uncertainties in the surface pressure ($\pm$10 mb) for the Skukuza site

Central Wavelength (nm)		470	550	645	870	1,240	1,650	2,130
Surface Reflectance $\times$ 10,000		400	636	800	2,226	2,880	2,483	1,600
Maximum Error $\times$ 10,000	Clear	0004i	0002e	0006i	0009i	0007i	0006i	0005i
	Avg.	0004i	0002e	0006i	0009i	0007i	0006i	0005j
	High	0003i	0001e	0006i	0009i	0007i	0005i	0005i
Minimum Error $\times$ 10,000	Clear	0000j	0000a	0000a	0000a	0000a	0000a	0000a
	Avg.	0000j	0000a	0000a	0000a	0000a	0000a	0000a
	High	0000c	0000a	0000a	0000a	0000a	0000a	0000a
Average Error $\times$ 10,000	Clear	1	0	1	1	0	1	1
	Avg.	1	0	1	1	0	1	1
	High	0	0	1	1	0	1	1

Table 8.3(c) Error on the surface reflectance (× 10,000) due to uncertainties in the
surface pressure (±10 mb) for the Sevilleta site

Central Wavelength (nm)		470	550	645	870	1,240	1,650	2,130
Surface Reflectance × 10,000		700	1,246	1,400	2,324	2,929	3,085	2,800
Maximum Error × 10,000	Clear	0005i	0002d	0003i	0007i	0005i	0002i	0004j
	Avg.	0004i	0002d	0003i	0006i	0005i	0002i	0003f
	High	0004i	0002e	0003i	0006i	0005i	0002i	0003j
Minimum Error × 10,000	Clear	0001a	0001a	0000b	0000a	0000a	0000a	0001i
	Avg.	0000j	0000b	0000a	0000a	0000a	0000a	0000i
	High	0000a	0000a	0000a	0000a	0000a	0000a	0000i
Average Error × 10,000	Clear	1	1	1	0	0	0	2
	Avg.	1	1	1	0	0	0	1
	High	1	1	0	0	0	0	1

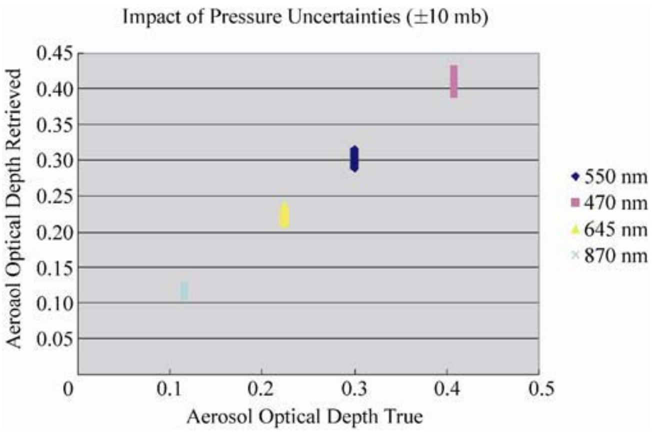

Figure 8.4 Comparison of the optical depth at 470 nm, 550 nm, 645 nm and 870 nm retrieved and input in the simulation for the 9 geometries given in Table 8.2 for an error on the surface pressure of ±10 mb

8.5.3 Uncertainties on Ancillary Ozone Amount

We ran a set of simulations at three different ozone contents, 0.25 cm.atm, 0.30 cm.atm, and 0.30 cm.atm, with a variation of 0.02 cm.atm for each case for an optical depth of 0.3. Tables 8.4(a) – 8.4(c) report the error in each band for the three different sites. The uncertainties on ozone most affect the band at 550 nm, but the impact is relatively small when comparing to calibration uncertainties. However, since the band at 470 nm is also affected the aerosol optical retrieved (see Fig. 8.5) is impacted.

Table 8.4(a) Error on the surface reflectance ($\times$ 10,000) due to uncertainties in the ozone content ($\pm$0.02 cm.atm) for the Belterra site

Central Wavelength (nm)		470	550	645	870	1,240	1,650	2,130
Surface Reflectance $\times$ 10,000		120	375	240	2,931	3,083	1,591	480
Maximum Error $\times$ 10,000	Clear	0001g	0022j	0006i	0019j	0009j	0010i	0011i
	Avg.	0001g	0022j	0006i	0019j	0009j	0010i	0010i
	High	0001g	0022j	0006i	0019j	0009j	0010i	0010i
Minimum Error $\times$ 10,000	Clear	0000a	0002a	0000c	0000a	0000a	0000c	0000c
	Avg.	0000a	0002a	0000c	0000a	0000a	0000c	0000c
	High	0000a	0002a	0000c	0000a	0000a	0000c	0000c
Average Error $\times$ 10,000	Clear	0	7	1	3	1	2	3
	Avg.	0	7	1	3	1	2	3
	High	0	7	1	3	1	2	3

Table 8.4(b) Error on the surface reflectance ($\times$ 10,000) due to uncertainties in the ozone content ($\pm$0.02 cm.atm) for the Skukuza site

Central Wavelength (nm)		470	550	645	870	1,240	1,650	2,130
Surface Reflectance $\times$ 10,000		400	636	800	2,226	2,880	2,483	1,600
Maximum Error $\times$ 10,000	Clear	0002i	0021j	0005i	0024j	0012i	0011i	0011i
	Avg.	0002i	0021j	0005i	0023j	0012i	0011i	0011i
	High	0002i	0021j	0005i	0023j	0012i	0011i	0011i
Minimum Error $\times$ 10,000	Clear	0000j	0002a	0000c	0001c	0000a	0000a	0000c
	Avg.	0000j	0002a	0000c	0001c	0000a	0000a	0000c
	High	0000j	0002a	0000c	0001c	0000a	0000a	0000c
Average Error $\times$ 10,000	Clear	1	6	1	6	2	2	3
	Avg.	1	6	1	6	2	2	3
	High	1	6	1	6	2	2	3

Table 8.4(c) Error on the surface reflectance ($\times$ 10,000) due to uncertainties in the ozone content ($\pm$0.02 cm.atm) for the Sevilleta site

Central Wavelength (nm)		470	550	645	870	1,240	1,650	2,130
Surface Reflectance $\times$ 10,000		700	1,246	1,400	2,324	2,929	3,085	2,800
Maximum Error $\times$ 10,000	Clear	0004d	0024j	0011i	0030i	0024i	0018i	0014i
	Avg.	0004d	0024j	0011i	0030i	0024i	0018i	0014i
	High	0004d	0024j	0011i	0030i	0024i	0018i	0014i
Minimum Error $\times$ 10,000	Clear	0001e	0003a	0000c	0002c	0001a	0000a	0000a
	Avg.	0000j	0003a	0000c	0002c	0001a	0000a	0000a
	High	0000j	0003a	0000c	0002c	0001a	0000a	0000a
Average Error $\times$ 10,000	Clear	2	8	3	10	5	4	3
	Avg.	2	8	3	10	5	4	3
	High	2	8	3	10	5	4	3

This uncertainty affects all the bands, especially at 870 nm where the aerosol impact is important and extrapolated from 470 nm and 645 nm retrieval.

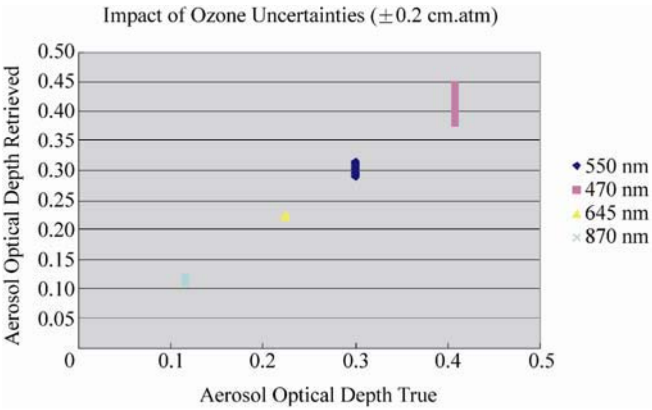

Figure 8.5 Comparison of the optical depth at 470 nm, 550 nm, 645 nm and 870 nm retrieved and input in the simulation for the 9 geometries given in Table 8.2 for an error on the ozone content of $\pm$0.02 cm.atm

8.5.4 Uncertainties on the Water Vapor Amount

The MODIS atmospheric correction algorithm uses the values of water vapor retrieved from differential absorption technique in the near-infrared which accuracy is better than 0.2 g/cm^2. To study the impact of the possible error on the water vapor amount, we ran a set of simulations at three different water vapor contents, 1 g/cm^2, 3 g/cm^2 and 5 g/cm^2, with a variation of 0.2 g/cm^2 for each case for an optical depth of 0.3. Tables 8.5(a) – 8.5(c) report the error in each band for the three different sites.

Table 8.5(a) Error on the surface reflectance ($\times$ 10,000) due to uncertainties in the water vapor content ($\pm 0.2\ \mathrm{g/cm^2}$) for the Belterra site

Central Wavelength (nm)		470	550	645	870	1,240	1,650	2,130
Surface Reflectance $\times$ 10,000		120	375	240	2,931	3,083	1,591	480
Maximum Error $\times$ 10,000	Clear	0001d	0002i	0004i	0007i	0004i	0002i	0006i
	Avg.	0001i	0001b	0003i	0005i	0003i	0001d	0004i
	High	0001i	0001d	0003i	0005i	0003i	0001i	0003i
Minimum Error $\times$ 10,000	Clear	0000a	0000j	0001c	0004a	0002a	0000a	0003a
	Avg.	0000a	0000a	0001a	0003a	0001a	0000a	0002a
	High	0000a	0000a	0001a	0002a	0001a	0000a	0001c
Average Error $\times$ 10,000	Clear	0	1	2	5	2	0	3
	Avg.	0	0	1	3	1	0	2
	High	0	0	1	3	1	0	2

Table 8.5(b) Error on the surface reflectance ($\times$ 10,000) due to uncertainties in the water vapor content ($\pm 0.2\ \mathrm{g/cm^2}$) for the Skukuza site

Central Wavelength (nm)		470	550	645	870	1,240	1,650	2,130
Surface Reflectance $\times$ 10,000		400	636	800	2,226	2,880	2,483	1,600
Maximum Error $\times$ 10,000	Clear	0006j	0009d	0015i	0015i	0011i	0006i	0030i
	Avg.	0004j	0005b	0009d	0009i	0006i	0003i	0018i
	High	0003j	0004d	0007g	0007i	0005i	0003i	0014i
Minimum Error $\times$ 10,000	Clear	0001a	0003a	0005a	0004c	0001c	0000c	0010c
	Avg.	0001a	0002a	0003a	0003a	0001a	0000a	0006c
	High	0000a	0001a	0003a	0002a	0001a	0000a	0005a
Average Error $\times$ 10,000	Clear	2	4	6	6	2	1	13
	Avg.	1	2	4	4	1	0	8
	High	1	1	3	3	1	0	6

Table 8.5(c) Error on the surface reflectance ($\times$ 10,000) due to uncertainties in the water vapor content ($\pm 0.2\ g/cm^2$) for the Sevilleta site

Central Wavelength (nm)		470	550	645	870	1,240	1,650	2,130
Surface Reflectance × 10,000		700	1,246	1,400	2,324	2,929	3,085	2,800
Maximum Error × 10,000	Clear	0004d	0024j	0011i	0030i	0024i	0018i	0014i
	Avg.	0004d	0024j	0011i	0030i	0024i	0018i	0014i
	High	0004d	0024j	0011i	0030i	0024i	0018i	0014i
Minimum Error × 10,000	Clear	0001a	0005a	0008c	0005c	0000c	0000a	0015c
	Avg.	0001a	0004a	0006a	0004c	0000f	0000a	0010c
	High	0001a	0003a	0004c	0003c	0000c	0000a	0008c
Average Error × 10,000	Clear	3	7	11	9	4	1	21
	Avg.	2	4	7	6	2	0	13
	High	1	3	5	4	2	0	10

The band at 2,130 nm is the most affected by the error on water vapor, there is some small impact at 645 nm and 870 nm. Since 2,130 nm is affected, an error will impact the aerosol retrieval (see Fig. 8.6) and therefore all the band to a lesser extent.

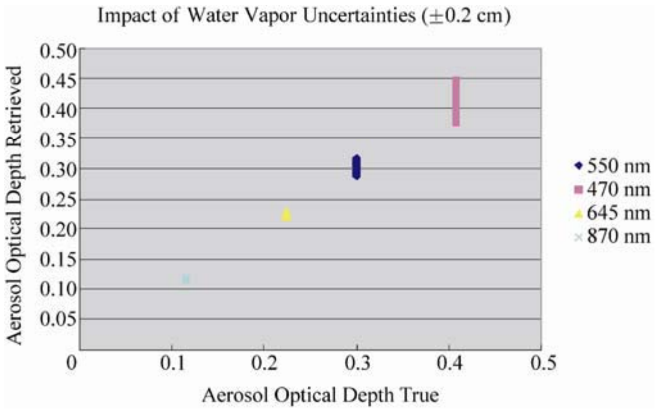

Figure 8.6 Comparison of the optical depth at 470 nm, 550 nm, 645 nm and 870 nm retrieved and input in the simulation for the 9 geometries given in Table 8.2 for an error on the water vapor content of $\pm 0.2\ g/cm^2$

8.5.5 Uncertainties on Empirical Relationship used to Determine the Surface Reflectance at 470 nm and 645 nm

The MODIS atmospheric correction algorithm uses an empirical relationship to predict the reflectance at 470 nm and 645 nm from the reflectance observed at 2,130 nm (Vermote et al., 2002), following the aerosol retrieval approach over land adopted by the atmosphere group (Kaufman et al., 1997). To account for deviation from this relationship we consider error of 0.005 in the surface estimation at 470 nm and 645 nm and run the atmospheric correction algorithm for three sites, at three different optical depths and in the nine geometries given in Table 8.1(a). The impact of the uncertainties in the empirical relationship is summarized in Tables 8.6(a) – 8.6(c). Figure 8.7 shows the impact on the retrieved optical thickness.

Table 8.6(a) Error on the surface reflectance (× 10,000) due to uncertainties in the empirical relationship between 2,130 nm and 470 nm, 645 nm for the Belterra site

Central Wavelength (nm)		470	550	645	870	1,240	1,650	2,130
Surface Reflectance × 10,000		120	375	240	2,931	3,083	1,591	480
Maximum Error × 10,000	Clear	0056j	0056j	0057a	0026j	0025f	0034b	0055a
	Avg.	0052a	0055j	0064a	0029j	0016i	0024b	0029b
	High	0053d	0063d	0066a	0029j	0018i	0027i	0027a
Minimum Error × 10,000	Clear	0050c	0044f	0049e	0003a	0000a	0000f	0024e
	Avg.	0050h	0050d	0053j	0002c	0002a	0005c	0007e
	High	0050j	0052h	0051e	0000d	0002a	0005e	0003j
Average Error × 10,000	Clear	52	49	52	10	11	17	37
	Avg.	51	52	57	9	6	13	17
	High	51	56	58	10	6	13	16

Table 8.6(b) Error on the surface reflectance (× 10,000) due to uncertainties in the empirical relationship between 2,130 nm and 470 nm, 645 nm for the Skukuza site

Central Wavelength (nm)		470	550	645	870	1,240	1,650	2,130
Surface Reflectance × 10,000		400	636	800	2,226	2,880	2,483	1,600
Maximum Error × 10,000	Clear	0056j	0057j	0060a	0039i	0037f	0038b	0066b
	Avg.	0052a	0061a	0069a	0036i	0025i	0023i	0030b
	High	0054d	0072d	0073a	0039i	0027i	0026i	0027b
Minimum Error × 10,000	Clear	0049c	0048c	0047e	0001f	0004e	0001e	0002f
	Avg.	0050f	0056h	0052j	0011f	0003e	0001e	0003c
	High	0051a	0054h	0051e	0015f	0002c	0001c	0003e
Average Error × 10,000	Clear	52	52	52	21	16	19	31
	Avg.	51	58	60	25	10	10	13
	High	51	62	62	27	10	10	14

Table 8.6(c) Error on the surface reflectance (× 10,000) due to uncertainties in the empirical relationship between 2,130 nm and 470 nm, 645 nm Sevilleta site

Central Wavelength (nm)		470	550	645	870	1,240	1,650	2,130
Surface Reflectance × 10,000		700	1,246	1,400	2,324	2,929	3,085	2,800
Maximum Error × 10,000	Clear	0056j	0056j	0063b	0056b	0088f	0172f	0183f
	Avg.	0052b	0064g	0076a	0058b	0038i	0030f	0027f
	High	0053d	0074d	0088g	0059i	0044i	0034i	0026i
Minimum Error × 10,000	Clear	0049c	0044c	0045e	0005f	0006a	0003d	0001a
	Avg.	0050f	0055h	0052j	0017f	0004e	0001a	0001e
	High	0050a	0053h	0050j	0022f	0004c	0000h	0000e
Average Error × 10,000	Clear	51	47	52	29	29	41	42
	Avg.	51	59	65	37	17	13	11
	High	51	63	68	39	18	12	10

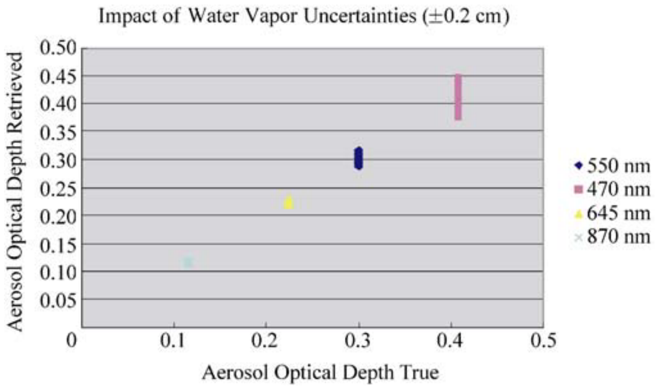

Figure 8.7 Comparison of the optical depth at 470 nm, 550 nm, 645 nm and 870 nm retrieved and input in the simulation for the 9 geometries given in Table 8.1(a) for an error of the estimation of the surface reflectance at 470 nm and 645 nm of 0.005 (empirical relationship)

8.5.6 Uncertainties on the Aerosol Model

The aerosol model is fixed to the urban clean case; it is possible to prescribe the model of aerosol as it is suggested by Kaufman et al., depending on the geographic location. However, the actual model may differ significantly from the actual aerosol. Tables 8.7(a) – 8.7(c) to 8.9(a) – 8.9(c) give an idea of the error generated by the use of the improper model. We simulated the error for three additional models, urban polluted cases, a smoke low and smoke high absorption case.

Figure 8.8 shows the associated error on the aerosol optical thickness for the smoke low absorption case, in this case the model is close to the assumed one; however, the error on the optical thickness is significant. Tracking the optical thickness is part of the validation process and enables us to estimate on a global basis the error introduced by the uncertainty on the model.

Table 8.7(a) Error on the surface reflectance ($\times$ 10,000) due to uncertainties in the aerosol model assumption (here smoke low absorption) for the Belterra site

Central Wavelength (nm)		470	550	645	870	1,240	1,650	2,130
Surface Reflectance × 10,000		120	375	240	2,931	3,083	1,591	480
Maximum Error × 10,000	Clear	0019j	0027j	0039j	0046j	0059j	0078j	0099j
	Avg.	0017i	0019j	0028i	0126j	0102j	0074j	0065j
	High	0043i	0068i	0116i	0230i	0197i	0200i	0176i
Minimum Error × 10,000	Clear	0000a	0000b	0000b	0002c	0000f	0000f	0001b
	Avg.	0000b	0003b	0000a	0050c	0033c	0013b	0000b
	High	0000b	0004a	0004f	0080a	0054b	0017b	0002e
Average Error × 10,000	Clear	2	4	5	12	10	10	13
	Avg.	4	9	7	75	52	28	16
	High	8	19	21	123	91	53	30

Table 8.7(b) Error on the surface reflectance ($\times$ 10,000) due to uncertainties in the aerosol model assumption (here smoke low absorption) for the Skukuza site

Central Wavelength (nm)		470	550	645	870	1,240	1,650	2,130
Surface Reflectance × 10,000		400	636	800	2,226	2,880	2,483	1,600
Maximum Error × 10,000	Clear	0017j	0024j	0034j	0048j	0059j	0069j	0087j
	Avg.	0018j	0008j	0019j	0089j	0092j	0076j	0065j
	High	0027i	0045i	0104i	0213i	0188i	0161i	0131i
Minimum Error × 10,000	Clear	0000a	0000b	0000f	0002c	0001f	0000f	0001c
	Avg.	0002a	0000f	0000b	0033a	0028b	0016b	0003b
	High	0002b	0000a	0001d	0042b	0042b	0023b	0001b
Average Error × 10,000	Clear	1	2	5	10	10	9	11
	Avg.	5	2	6	50	46	31	17
	High	9	10	17	86	82	57	32

Table 8.7(c) Error on the surface reflectance (× 10,000) due to uncertainties in the aerosol model assumption (here smoke low absorption) for the Sevilleta site

Central Wavelength (nm)		470	550	645	870	1,240	1,650	2,130
Surface Reflectance × 10,000		700	1,246	1,400	2,324	2,929	3,085	2,800
Maximum Error × 10,000	Clear	0015j	0021j	0030j	0046j	0057j	0064j	0076j
	Avg.	0020j	0021j	0020j	0071j	0084j	0077j	0067j
	High	0020j	0038i	0053i	0127i	0119i	0094i	0060i
Minimum Error × 10,000	Clear	0000a	0001c	0001c	0002c	0002c	0002c	0001f
	Avg.	0005a	0009c	0007d	0028b	0025b	0021b	0012b
	High	0004b	0017g	0002d	0041b	0041b	0033b	0018b
Average Error × 10,000	Clear	1	4	6	10	9	10	10
	Avg.	8	13	10	41	42	36	25
	High	10	26	17	67	73	60	40

Table 8.8(a) Error on the surface reflectance (× 10,000) due to uncertainties in the aerosol model assumption (here urban polluted) for the Belterra site

Central Wavelength (nm)		470	550	645	870	1,240	1,650	2,130
Surface Reflectance × 10,000		120	375	240	2,931	3,083	1,591	480
Maximum Error × 10,000	Clear	0019j	0017j	0021j	0053j	0054j	0051j	0053j
	Avg.	0025i	0044j	0081j	0255i	0175i	0090i	0086j
	High	0033j	0053d	0089j	0363i	0258i	0125d	0153j
Minimum Error × 10,000	Clear	0000a	0000b	0000a	0017c	0013c	0004b	0001a
	Avg.	0000a	0006e	0000a	0123a	0083b	0006j	0001a
	High	0000a	0016b	0001c	0197a	0137b	0015j	0001a
Average Error × 10,000	Clear	1	3	3	27	21	11	7
	Avg.	6	17	15	166	118	42	17
	High	8	29	28	272	194	73	35

Table 8.8(b) Error on the surface reflectance (× 10,000) due to uncertainties in the aerosol model assumption (here urban polluted) for the Skukuza site

Central Wavelength (nm)		470	550	645	870	1,240	1,650	2,130
Surface Reflectance × 10,000		400	636	800	2,226	2,880	2,483	1,600
Maximum Error × 10,000	Clear	0008j	0012j	0020j	0043j	0050j	0049j	0047j
	Avg.	0022i	0053j	0060j	0157i	0129i	0082f	0049j
	High	0019c	0055j	0057j	0251i	0227i	0145i	0091j
Minimum Error × 10,000	Clear	0000a	0001b	0002c	0013c	0013b	0008b	0000i
	Avg.	0004b	0000e	0000b	0069j	0067b	0027j	0003b
	High	0003b	0005h	0006b	0117b	0109b	0039j	0005b
Average Error × 10,000	Clear	1	2	4	20	19	14	8
	Avg.	8	8	15	105	102	62	25
	High	13	13	20	172	168	102	44

Table 8.8(c) Error on the surface reflectance (× 10,000) due to uncertainties in the aerosol model assumption (here urban polluted) for the Sevilleta site

Central Wavelength (nm)		470	550	645	870	1,240	1,650	2,130
Surface Reflectance × 10,000		700	1,246	1,400	2,324	2,929	3,085	2,800
Maximum Error × 10,000	Clear	0006j	0014j	0018j	0037j	0046j	0046j	0043j
	Avg.	0026i	0058g	0059f	0123f	0126f	0110f	0081j
	High	0032e	0078f	0078f	0188f	0199f	0175f	0128f
Minimum Error × 10,000	Clear	0000i	0005h	0005e	0014c	0013b	0011b	0007b
	Avg.	0000j	0012j	0020i	0043j	0068b	0048j	0007j
	High	0000j	0011j	0020j	0106j	0110b	0072j	0022j
Average Error × 10,000	Clear	1	9	10	20	20	17	13
	Avg.	15	41	41	94	97	82	52
	High	22	60	56	153	158	131	85

Table 8.9(a) Error on the surface reflectance (× 10,000) due to uncertainties in the aerosol model assumption (here smoke high absorption) for the Belterra site

Central Wavelength (nm)		470	550	645	870	1,240	1,650	2,130
Surface Reflectance × 10,000		120	375	240	2,931	3,083	1,591	480
Maximum Error × 10,000	Clear	0015j	0022j	0029j	0069j	0069j	0065j	0067j
	Avg.	0058i	0091i	0131i	0365i	0289i	0260i	0257i
	High	0043d	0143i	0240i	0495j	0345j	0247g	0222g
Minimum Error × 10,000	Clear	0000a	0002b	0000b	0020c	0015c	0006c	0001b
	Avg.	0001e	0013j	0000e	0146a	0103b	0041b	0007b
	High	0003c	0008j	0000e	0237a	0170a	0027i	0001j
Average Error × 10,000	Clear	2	5	5	33	25	15	11
	Avg.	10	29	25	211	154	82	43
	High	15	57	59	332	237	114	60

Table 8.9(b) Error on the surface reflectance (× 10,000) due to uncertainties in the aerosol model assumption (here smoke high absorption) for the Skukuza site

Central Wavelength (nm)		470	550	645	870	1,240	1,650	2,130
Surface Reflectance × 10,000		400	636	800	2,226	2,880	2,483	1,600
Maximum Error × 10,000	Clear	0013j	0017j	0027j	0057j	0064j	0061j	0060j
	Avg.	0037i	0030j	0050i	0207i	0180i	0128i	0075i
	High	0032i	0040i	0054g	0313j	0295j	0179j	0089g
Minimum Error × 10,000	Clear	0000b	0001i	0003c	0015c	0016b	0010b	0004b
	Avg.	0007b	0001e	0006b	0093b	0084b	0051b	0014b
	High	0006c	0000b	0003b	0148b	0137b	0082b	0023b
Average Error × 10,000	Clear	2	3	6	24	23	18	12
	Avg.	13	11	19	136	130	87	40
	High	18	17	26	220	212	140	63

Table 8.9(c) Error on the surface reflectance (× 10,000) due to uncertainties in the aerosol model assumption (here smoke high absorption) for the Sevilleta site

Central Wavelength (nm)		470	550	645	870	1,240	1,650	2,130
Surface Reflectance × 10,000		700	1,246	1,400	2,324	2,929	3,085	2,800
Maximum Error × 10,000	Clear	0011j	0019j	0026j	0050j	0060j	0058j	0055j
	Avg.	0030i	0073g	0071f	0140f	0159j	0130j	0087f
	High	0047i	0098f	0098f	0250j	0267j	0208j	0140f
Minimum Error × 10,000	Clear	0001c	0007e	0007e	0016c	0016b	0013b	0009b
	Avg.	0014c	0014j	0006j	0095b	0085b	0070b	0045b
	High	0018b	0055j	0052j	0150b	0136b	0111b	0072b
Average Error × 10,000	Clear	2	12	13	24	24	21	16
	Avg.	20	52	48	121	122	104	72
	High	31	83	77	200	203	172	118

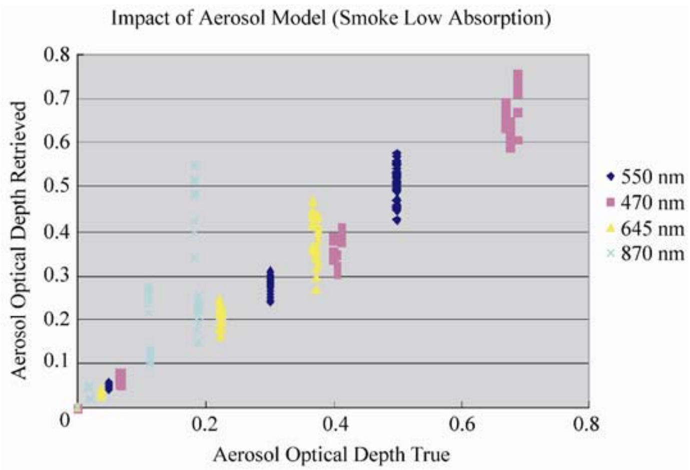

Figure 8.8 Comparison of the optical depth at 470 nm, 550 nm, 645 nm and 870 nm retrieved and input in the simulation for the 9 geometries and 3 optical depths given in Table 8.1(a) for an error on the aerosol model (actual smoke low absorption versus the urban clean used in the inversion)

Given the fact that under our assumption this error dominates any other sources, the choice of the aerosol model is critical to improve the theoretical accuracy of the current product and in particular the accuracy of the optical thickness retrieved. The dependence of the model used based on the geographic location is a first step in that direction, but one can imagine further steps involving use of aerosol and transport model such as GOCART (Chin et al., 2002) to determine the model or an attempt to invert the aerosol model using additional wavelength (i.e. 412 nm and 443 nm).

8.5.7 Overall Uncertainties

An overall uncertainty was estimated by computing the quadratic average of each average error generated by the uncertainties considered in 8.5.1 – 8.5.6 for each site. The results are presented in Table 8.10. The overall accuracy can be summarized under this term, in clear condition the average accuracy is 0.006 reflectance units or 5% relative whatever is higher, in average condition the average accuracy is 0.007 reflectance units or 7% relative whatever is higher, and in high aerosol loading conditions the average accuracy is 0.007 reflectance units or 9% relative whatever is higher. However, the minimum and maximum error observed for each category suggest a strong dependence of the error with the geometrical conditions, we are therefore planning in future version of the surface reflectance product (Collection 5 and 6) to introduce pixels and band dependent estimate of the accuracy.

Table 8.10 Overall theoretical accuracy of the atmospheric correction method considering the error source on calibration, ancillary data and aerosol inversion for 3 aerosol optical thickness (0.05: clear, 0.3: avg., 0.5: high). The uncertainties are considered independent and summed in quadratic

Central Wavelength (nm)		470	550	645	870	1,240	1,650	2,130
Belterra	Surface Reflectance × 10,000	120	375	240	2,931	3,083	1,591	480
	Clear	52	50	53	67	69	49	52
	Avg.	51	55	59	163	124	61	32
	High	52	64	65	255	189	92	46
Skukuza	Surface Reflectance × 10,000	400	636	800	2,226	2,880	2,483	1,600
	Clear	53	54	55	57	65	61	57
	Avg.	52	60	64	114	113	81	49
	High	53	64	70	174	169	116	64
Sevilleta	Surface Reflectance × 10,000	700	1,246	1,400	2,324	2,929	3,085	2,800
	Clear	53	54	61	61	70	79	78
	Avg.	55	74	79	108	109	99	78
	High	56	88	90	158	161	139	102

8.5.8 Validation of the Atmospheric Correction Algorithm

The validation of the atmospheric correction involves the validation of the atmospheric parameters used in the correction and the validation of the surface reflectance's themselves by comparison to surface reflectance estimates (derived from the use of sun-photometers data and validated against surface measurements of reflectance via high spatial resolution sensor such as ETM+. More details on the validation can be found in Vermote el al. (2002) and will not be discussed here. So far the validation has confirmed the validity of the theoretical error budget presented here but need to be extended to cover more conditions. This effort will be conducted during the validation stage 2 and 3 (Morisette et al., 2002).

8.6 Conclusions

The general approach for operational correction of the remotely sensed data in the visible to shortwave infrared spectral region assuming an infinite Lambertian target has been presented in detail. A detailed error budget has been presented in the case of the MODIS sensor. Overall, the accuracy of the atmospheric correction process has been confirmed by the validation effort which is still on-going. The error budget needs to be updated when considering non-uniform and non- Lambertian surface's as the algorithm to handle those effects becomes mature. However, the influence of those effects is probably of the second order (Vermote and Vermeulen. MODIS Atmospheric correction over land: surface reflectance, Algorithm Theoretical Basis Document. 1999, http:// modis.gsfc.nasa.gov/data/ atbd/atbd_mod08.pdf).

The accuracy is highly variable with respect to the geometrical conditions, the aerosol loading and the spectral band considered. The future version of the reflectance product will include a theoretical uncertainty estimate on a pixel, band basis.

The error budget points to the fact that improvement needs to be made in the area of the aerosol model used in the correction, especially accounting for the absorption of aerosol. This issue needs to be addressed to further reduce the uncertainties and several options are available.

References

Chin M et al. (2002) Tropospheric aerosol optical thickness from the GOCART model and comparisons with satellite and sunphotometer measurements. J Atmos Sci 59: 461 – 483

Deschamps PY, Herman M, Tanre D (1983) Modeling of the atmospheric effects and its applications to the remote sensing of ocean color. Appl Optics 22: 3,751 – 3,758

Dubovik O, Holben BN, Eck TF, Smirnov A, Kaufman YJ, King MD, Tanre D, Slutsker I (2002) Variability of absorption and optical properties of key aerosol types observed in worldwide locations. J Atm Sci 59: 590 – 608

El Saleous NZ, Vermote EF, Justice CO, Townshend JRG, Tucker CJ, Goward SN (2000) Improvements in the global biospheric record from the Advanced Very High Resolution Radiometer (AVHRR). International Journal of Remote Sensing 21(6): 1,251 – 1,277

Gao BC, Kaufman YJ (2003) Water vapor retrievals using Moderate Resolution Imaging Spectroradiometer (MODIS) near-infrared channels. Journal of Geophysical Research 108(D13), doi. 10.1029

Gordon HR, Clark DK, Brown JW, Brown OB, Evans RH, Broenkow WW (1983) Phytoplankton pigment concentrations in the Middle Atlantic Bight: comparison of ship determinations and CZCS estimates. Appl Optics 22: 20 – 36

Holben BN, Vermote EF, Kaufman YJ, Tanré D, Kalb V (1992) Aerosol Retrieval over Land from AVHRR data-Application for Atmospheric Correction. IEEE Transaction on Geoscience and Remote Sensing 30(2): 212 – 222

James ME, Kalluri SNV (1994) The Pathfinder AVHRR Land Data Set - An Improved Coarse Resolution Data Set For Terrestrial Monitoring. International Journal of Remote Sensing 15(17): 3,347 – 3,363

Kaufman YJ, Tanré D, Remer L, Vermote EF, Chu A, Holben BN (1997) Operational Remote Sensing of Tropospheric Aerosol Over the Land from EOS-MODIS. Journal of Geophysical Research 102(D14): 17,051 – 17,068

Martonchik J (1997) Determination of aerosol optical depth and land surface directional reflectances using multi-angle imagery. J Geophys Res Atmos 102: 17,015 – 17,022

Morisette JT, Privette JL, Justice CO (2002) A framework for the validation of MODIS land products. Remote Sensing of Environment 83(1-2): 77 – 96

Ouaidrari H, Vermote EF (1999) Operational Atmospheric Correction of Landsat TM data. Remote Sensing of the Environment 70: 4 – 15

Vermote EF, Tanré D (1992) Analytical Expressions for Radiative Properties of Planar Rayleigh Scattering Media Including Polarization Contribution. Journal of Quantitative Spectroscopy and Radiative Transfer 47(4): 305 – 314

Vermote EF, Tanré D, Deuzé JL, Herman M, Morcrette JJ (1997) Second simulation of the satellite signal in the solar spectrum (6S). Users Guide Version 2.0. Department of Geography, University of Maryland, Laboratoire d'Optique Atmosphérique, U.S.T.L., p 218

Vermote EF, El Saleous NZ, Justice CO, Kaufman YJ, Privette JL, Remer L, Roger JC, Tanre D (1997) Atmospheric correction of visible to middle-infrared EOS-MODIS data over land surfaces: Background, operational algorithm and validation. Journal of Geophysical Research Atmosphere 102 (D14): 17,131 – 17,141

Vermote EF, Justice CO, Descloitres J, El Saleous NZ, Ray J, Roy D, Margerin B, Gonzalez L (2001) A global monthly coarse resolution reflectance data set from SeaWiFS for use in Land, Ocean and Atmosphere applications. International Journal of Remote Sensing 22(6): 1,151 – 1,158

Vermote EF, El Saleous NZ, Justice C (2002) Atmospheric correction of the MODIS data in the visible to middle infrared: First results. Remote Sensing of Environment 83(1-2): 97 – 111